optica

Metamorphic plasmonic nanoantennas for self-enhanced nonlinear light generation: supplementary material

KONRAD SCHRAML[1,2,+], ARMIN REGLER[1,3,+], JOHANNES BARTL[1], GLENN GLASHAGEN[1], JAKOB WIERZBOWSKI[1], JONATHAN J. FINLEY[1,2,3], AND MICHAEL KANIBER[1,*]

[1] Walter Schottky Institut and Physik Department, Technische Universität München, Am Coulombwall 4, 85748 Garching, Germany
[2] Nanosystems Initiative Munich, Schellingstraße 4, 80799 München, Germany
[3] TUM Institute of Advanced Study, Lichtenbergstraße 2a, 85748 Garching, Germany
[+] Those authors contributed equally.
[*] Corresponding author: michael.kaniber@wsi.tum.de

Published 5 December 2016

This document provides supplementary information to "Metamorphic plasmonic nanoantennas for self-enhanced nonlinear light generation," http://dx.doi.org/10.1364/OPTICA.3.001453. It contains further details on the sample fabrication, the confocal microscopy setup, spatially resolved two photon photoluminescence, additional SEM images of gap-particle bowties, temporally resolved integrated photoluminescence spectra of bowties with g = 20 nm, photoluminescence-spectra for different excitation powers, the calculation of the fill factor of a bowtie in the exciting laser spot, the calculation of the conversion efficiency, simulations of the intensity enhancement for different polarisations, simulations of the intensity enhancement as a function of feedgap size and simulations with varying particle numbers and shapes in the feedgap of a bowtie.

http://dx.doi.org/10.1364/optica.3.001453.s001

1. SAMPLE FABRICATION

The samples investigated were defined on glass (MENZEL microscope cover slips) substrates. First, the samples were flushed with acetone and isopropanol (IPA). In order to achieve superior adhesion properties of the e-beam resist, the samples were placed on a hot plate at 170° C for 5 min in order to evaporate any residual water or solvent. We spin-coat an e-beam resist (Polymethylmethacrylat 950 K, AR-P 679.02, ALLRESIST) at 4000 rpm for 40 s with an initial acceleration of 2000 rpm/s and bake out at 170° C for 300 s, which gives rise to a resist thickness of 70 ± 5 nm. In order to reduce charging of the sample with electrons during electron exposure, we evaporated 10 nm aluminium on top of the Polymethylmethacrylat layer. The samples were illuminated in a Raith E-line system using an acceleration voltage of 30 kV and an aperture size of 10 μm. Before every fabrication run, we performed and analysed a detailed dose test, since this crucial parameter depends strongly on the varying electron beam current. Typical values were 700 μC/cm^2. After the e-beam writing the aluminium layer on the glass samples was selectively removed by etching using a metal-ion-free photoresist developer (AZ 726 MIF, MicroChemicals). The samples were developed in Methylisobutylketon diluted with IPA (1:3) for 45 s. To stop the development, the sample was rinsed with pure IPA. For the metallisation we used an e-beam to deposit a 5 nm thick titanium adhesion layer, followed by a 35 nm gold layer at a low rate of 0.1 nm/s. The lift-off was performed in 50 ° warm acetone, leaving behind high-quality nanostructures with feature sizes on the order of 10 nm.

2. OPTICAL SPECTROSCOPY

The non-linear optical properties of individual nanoantennas were investigated in a home-build confocal photoluminescence microscope with a resolution limited spot of size ~ 1 μm. The sample was excited by spectrally tuneable (700 - 1000 nm), ultrashort (100 fs) laser pulses produced by a Titanium:Sapphire laser (Spectra Physics, Tsunami 3960-L3S), repetition rate (82 MHz) via an apochromatic high numerical aperture ($NA = 0.55$) microscope objective. The excitation polarisation was controlled

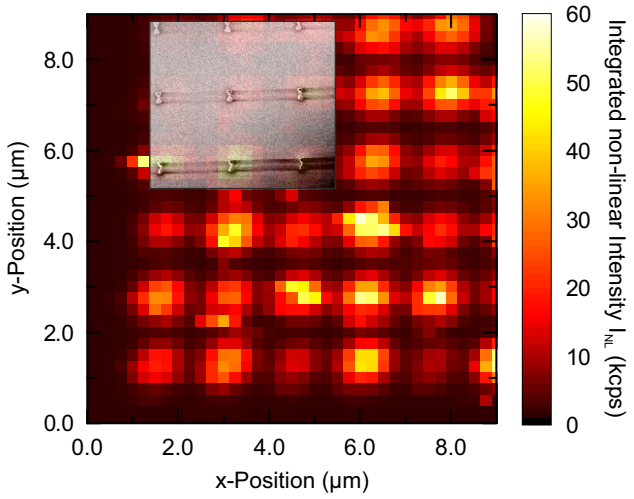

Fig. S1. Spatially resolved integrated photoluminescence map. Overlay shows SEM image of the scanned bowtie array

via a combination of $\lambda/2$-plate (Thorlabs, AHWP10M-980) and a broadband linear polariser (Thorlabs, LBVIS100-MP2), mounted on computer-controlled rotation stages (Thorlabs, PRM1/MZ8). The generated non-linear response from individual antennas was detected via the same microscopy objective and subsequently coupled into a multimode optical fibre and guided to a 0.5 m imaging spectrometer (Princeton Instruments Acton SP2500i, grating: 300l/mm), equipped with a Si-CCD camera (Princeton Instruments Spec-10). In order to suppressed the fundamental excitation beam we incorporated in the detection path two short-pass filters with a cut-on energy of 1.65 eV (Thorlabs, FESH0750). In order to avoid trapping of dust particle from the air, we placed the sample into a home-built vacuum chamber, enabling optical access via a glass window at a pressure of $< 2 \cdot 10^{-6}$ mbar. All measurement have been performed at room temperature $T \sim 300$ K.

In order to determine the plasmonic response of the individual nanoantennas before and after fs-illumination, we performed white light differential reflection spectroscopy using a similar setup geometry as described above. In order to excite individual antennas using broadband white light, we replaced the Titanium:Sapphire laser by a white-light super-continuum source (Fianium WhiteLase micro) and removed the short-pass filter in the detection path. To extract the differential reflection signal, we conducted reflectivity measurements spatially on R_{on} and spatially displaced (i.e. off) R_{off} the nanoantennas and calculated $\Delta R/R_{off} = (R_{on} - R_{off})/R_{off}$. Detailed structural and optical investigations of individual bowtie nanoantennas on both glass and GaAs substrate can be found in Ref. [1].

3. SPATIALLY RESOLVED TWO PHOTON PHOTOLUMINESCENCE

In order to demonstrate that the observed luminescence signal at energies $E > E_L$, where E_L denotes the fundamental laser energy, stems indeed from the plasmonic nanoantennas, we performed spatially resolved luminescence measurements by scanning the excitation spot across the sample surface at a constant excitation peak power density of $PPD = 2.33\,\mathrm{GW/cm^2}$. In figure S1, we present an example of such a spatially resolved measurements, where we encoded the spectrally integrated luminescence signal

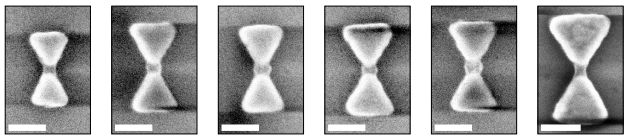

Fig. S2. SEM images of bowties after fs-illumination. Scale bar = 100 nm.

in colour. We clearly observe a periodic pattern of enhanced luminescence signal (i.e. bright spots) with a periodicity of $\sim 1.5\mu m$, matching the separation of two adjacent nanoantennas. The periodicity extracted from this optical measurement is found to be in excellent agreement with lattice constant extracted from scanning electron microscopy (SEM) measurement as shown by the overlaid image in figure S1. The strong fluctuation in the signal strength between nominally identically bowties observed in this measurement is attributed to the fact that the feedgaps of the individual bowtie nanoantennas slightly vary on the nanometre lengthscale and, moreover, that the used excitation power density during this initial illumination exceeded the destruction limit of the antennas. Nevertheless, the finding unambiguously demonstrates that the observed high-energy signal stems indeed from the nanoantennas and is attributed to the non-linear optical response of the antennas.

4. ADDITIONAL SEM IMAGES

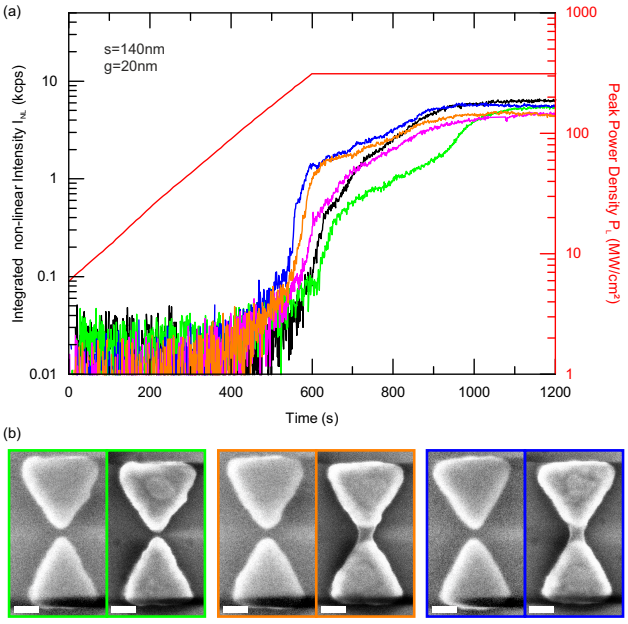

Fig. S3. (a) Temporal evolution of the integrated PL signal of bowties ($s = 140$ nm, $g = 20$ nm). (b) Selection of SEM images before and after the fs-illumination, respectively (Scale bar = 50 nm).

In figure S2, we present additional SEM images of bowties after fs-illumination. We clearly observe that material, supposedly Au, accumulates predominantly in the high electric field region of the antenna feedgap, in agreement with the field distribution for the near-field coupled mode as shown in figure S6

(a). We conclude that the electro-migration of the Au most likely appears due to the presence of the high plasmon induced field enhancement.

5. TEMPORALLY RESOLVED TWO-PHOTON PHOTOLUMINESCENCE

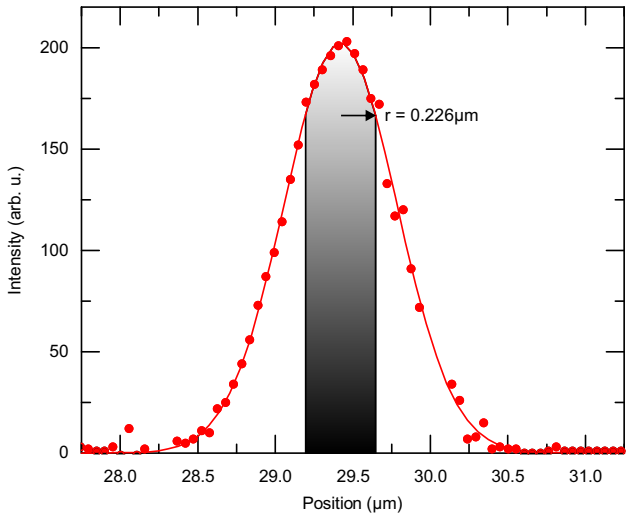

Fig. S5. Measured profile of the excitation laser spot on the sample surface.

Figure S3 (a) shows the temporal evolution of the integrated PL signal of bowties for gaps of $g = 20$ nm at an excitation power of PPD=312 MW/cm^2. Similar to Figure 3 (a) of the main text, the signal first rises quadratically at $t = 400$-500 s, before a sudden increases by one order of magnitude happens. Eventually, the non-linear signal converges to a constant value of $I_{sat} = 4000$-6000 cps for $t > 1000$ s. In S3 (b), we show the corresponding SEM images before and after the fs-illumination.

6. SPECTRALLY RESOLVED TWO-PHOTON PHOTOLUMINCESCENCE

In figure S4 (a), we show the same spectrally resolved two-photon photoluminescence (TPPL) spectra of a fs-illuminated antenna as in the main text of this manuscript (cp. Figure 3 (b)) for varying excitation power densities. As stated in the main part of this work, we did not observe any unusual spectral modifications of the TPPL spectrum for fixed excitation energy. In Figure S4 (b), we plot the TPPL intensity for four different detection energies and observe that the signal always follows a quadratic power law as indicated by the red line (guide-to-the-eye). Therefore, we conclude that we can study the overall non-linear response of the antennas by spectrally integrated the complete high-energy signal using a single photon counting module without loss of generality.

7. CALCULATION OF THE FILL FACTOR

The scattering cross-sections of sub-wavlength sized plasmonic nanoparticles are in general much smaller than the exciting laser spots in optical measurements, which have diameters of at least several hundreds of nanometers. In our case, this means that the bowtie interacts only with a certain fraction of the excitation light, whereas all photons hit the surface of the planar Au-film. In order to compare the conversion efficiencies of both systems, it is therefore necessary to normalise the TPPL to the number of photons interacting with the bowtie. Herefore, we experimentally determined the spatial extension of our laser spot by imaging the sample surface using a CCD camera. A cross-section through the center of the spot is plotted in Figure S5 together with an Gaussian fit of the data points. From the numerical simulations we obtain a scattering cross-sections for bowtie nanoantennas with $s = 140$ nm and $g = 10$ nm of 0.16 μm^2. Assuming a circularly shape excitation spot enables us to calculate the corresponding radius to be $0.226 \mu m$. By integrating an area of $\pm 0.226 \mu m$ in the center of the spot, we obtain a filling factor of 52% as shown in Figure S5. Consequently, the power dependent measurement of the TPPL from the fs-illuminated nanoantennas (cp. Figure 3 (c)) was corrected accordingly in order to state an accurate quantification of the intensity enhancement inside the antenna feedgap.

8. ESTIMATION OF THE CONVERSION EFFICIENCY

The conversion efficiency of $2.8 \cdot 10^{-7}$% was calculated in the following way; we measured the continuous wave-equivalent power after the beamsplitter of the used micro-photoluminescence setup to be $80 \mu W$. This corresponds to $1.35 \cdot 10^{15}$ photons being directed to the focusing objective at an energy of $E_{Phot} = 1.48$ eV. To calculate the maximum detectable photons for a conversion efficiency of 100%, we take the fill factor of the bowtie compared to the laser spot, the transmission properties of the used optics (i.e. objective, beamsplitter, mirrors, lenses) and the quantum efficiency of the used silicon detector into account. Since photons are emitted in every direction, but most likely perpendicular to the samples surface, we assumed that 50% of the emitted photons are again collected by the same microscope objective. This results in a maximum number of $2.5 \cdot 10^{13}$ photons, assuming that all photons would be converted into TPPL. However, since we detect only $7.0 \cdot 10^4$ photons, we can determine the conversion efficiency to be at least $2.8 \cdot 10^{-7}$%. We note that this value gives only a lower limit, since we cannot quantify the number of photons which we cut away with our shortpass filter.

9. NUMERICAL SIMULATIONS FOR DIFFERENT EXCITATION POLARISATION DIRECTIONS

Figure S6 shows FDTD simulations of the electric field intensity enhancement η of a bowtie under resonant excitation for different excitation polarisations. The result corresponds to an in-plane cut of the simulation cell 2 nm above the bowtie nanoantenna surface. When exciting with the polarisation direction along the bowtie axis (a) the strong near fields of the individual nanotriangles composing the bowtie nanoantenna overlap, leading to a coupling between the two particles. This coupled mode shows an extraordinary high η in the feedgap of $\eta \sim 1000$, whereas at the corners we observe only values of $\eta \sim 50$. By turning the excitation polarisation direction by 90°, the electrons oscillate along the outer edges of the bowtie nanoantenna. Here, the η at the corners are $\eta \sim 45$, whereas in the feedgap there is no significant intensity enhancement observed. Indeed, we obtain even lower values $\eta \sim 0.01$ than without the bowtie, which is five orders of magnitude lower than for a 0°-polarization. This phenomena allows us to switch the η in the feedgap region in a simple way.

10. ELECTRIC FIELD ENHANCEMENT VS. FEEDGAP SIZE

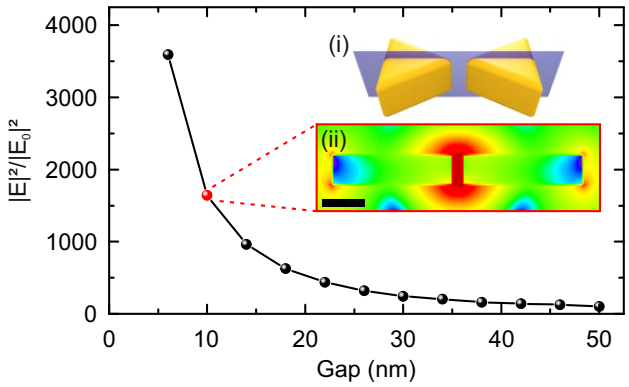

Fig. S7. FDTD simulation of the electric field intensity enhancement of a bowtie ($s = 140$ nm, $g = 10$ nm) at the electric dipole resonance as a function of feedgap size. (i) Sketch of the cross section shown in (ii) (scale bar = 50 nm).

In addition to the scattering spectra presented in Figure 1 (a) of the main text, we further calculated the electric field intensity enhancement η defined as the ratio of the intensities with ($|E|^2$) and without ($|E_0|^2$) the bowtie in our simulation environment. In particular, we evaluated the η at the cross-sections through the center of the bowties as indicated by the blue plane in inset (i) of Figure S7. The black curve is obtained by integrating the η over the region between the gold tips for different feedgap sizes. As expected from theory, the η increases as g decreases due the enhanced coupling between the two triangles. For $g = 6$ nm we obtain $\eta \sim 3500$ compared to $\eta \sim 100$ for $g = 50$ nm. The inset (ii) of Figure S7 shows an example of the distribution of the η for an antenna with $g = 10$ nm on a logarithmic scale. At the outer edges of the bowtie, we calculate values of only $\eta \sim 75$ directly at the corners, whereas within and around the feedgap the field is significantly enhanced and locally reaches values up to $\eta \sim 2500$. These numerical simulations suggest that the bowtie nanoantenna is able to provide a strong non-linear optical response.

11. NUMERICAL SIMULATIONS: NUMBER AND SHAPE OF PARTICLES IN THE GAP

In addition to the simulation presented in the main part of this work, we studied the influence of the shape and the number of particles on the η. Here, we integrated over the volume within the first 10 nm of the triangle tips composing a bowtie nanoantenna with $g = 10$ nm as indicated by the red highlighted tips of the inset in Figure S8. We calculated that the central particle increases the mean η from 104 to 16000. By adding two more particles we observe a value of $\eta = 16100$ whereas 6 additional particles do not have a significant effect on the η at all. Hence, we found that the central particle in the feed gap plays the major role, whereas the outer particles do not contribute significantly, which is in excellent agreement with the fact that the maximum intensity enhancement is located in the center of the feedgap. Moreover, we repeated the simulation with spherical particles of radius $r = 4$ nm. In analogue to the cylindrical particles the first sphere increases the η to 350, whereas 5 and 7 particles generate

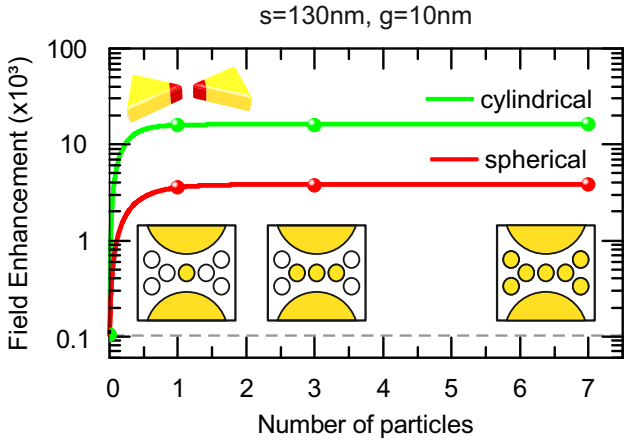

Fig. S8. FDTD simulations of the field enhancement in the tip of a bowtie for different shapes and number of particles in the feedgap.

a η of 380. The overall lower values of η for spheres compared to cylinders is most likely caused by their smaller volume.

REFERENCES

1. M. Kaniber, K. Schraml, A. Regler, J. Bartl, G. Glashagen, F. Flassig, and J. Wierzbowski, "Surface plasmon resonance spectroscopy of single bowtie nano-antennas using a differential reflectivity method," Sci. Rep. **6**, 23203 (2016).

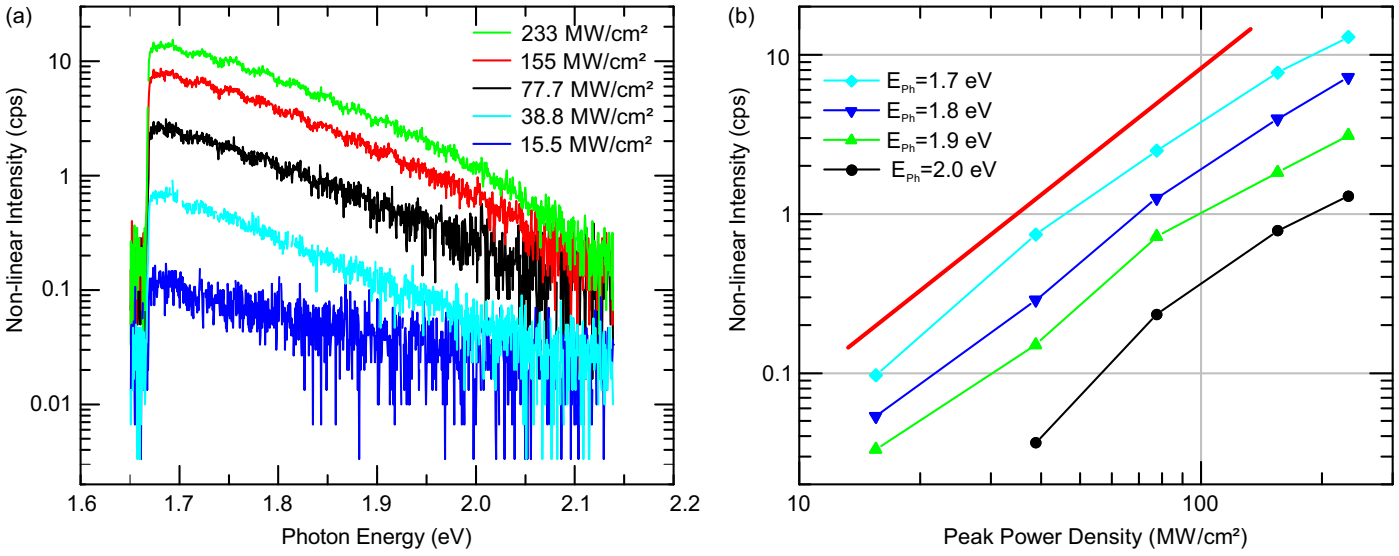

Fig. S4. (a) Two-photon photoluminescence spectra of pre-illuminated bowtie for different excitation powers. (b) Two-photon photoluminescence at certain photon energies as a function of excitation peak power density.

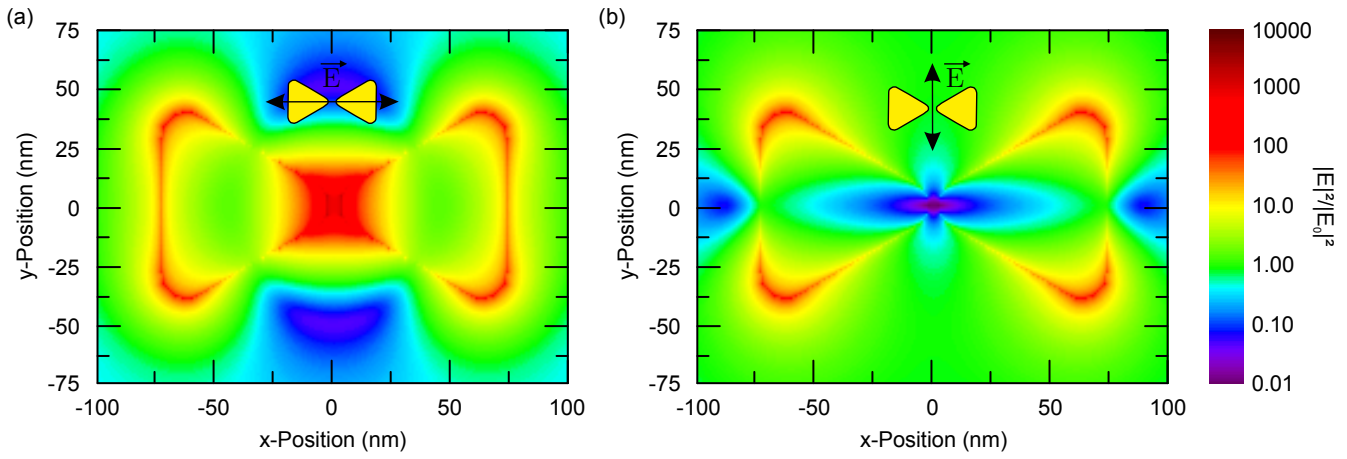

Fig. S6. FDTD simulations of the electric field intensity enhancement of a bowtie ($s = 140$ nm, $g = 10$ nm) at the electric dipole resonance for excitation along (a) and perpendicular (b) to the bowtie axis.